Published November, 2010

Special Section: Patterns

Christian N. Koyama
Wolfgang Korres
Peter Fiener
Karl Schneider*

Variability of Surface Soil Moisture Observed from Multitemporal C-Band Synthetic Aperture Radar and Field Data

The study aimed to analyze the spatial variability of surface soil moisture at different spatial scales based on field measurements and remote sensing estimates. Multitemporal Envisat satellite Advanced Synthetic Aperture Radar (ASAR) data were used to derive the surface soil moisture utilizing an empirical C-band retrieval algorithm. Eight wide-swath (WS) images with a spatial resolution of 150 m acquired between February and October 2008 were used to determine the surface soil moisture contents. The accuracy of the surface soil moisture retrievals was evaluated by comparison with in situ measurements. This comparison yielded a root mean square error of 5% (v/v). Based on our in situ measurements as well as remote sensing results, the relationship of the coefficient of variation of the spatial soil moisture patterns and the mean soil moisture was analyzed at different spatial scales ranging from the catchment scale to the field scale. Our results show that the coefficient of variation decreases at all scales with increasing soil moisture. The gain of this relationship decreases with scale, however, indicating that at a given soil moisture state, the spatial variation at the large scale of whole catchments is larger than at the field scale. Knowledge of the spatial variability of the surface soil moisture is important to better understand energy exchange processes and water fluxes at the land surface as well as their scaling properties.

Abbreviations: ASAR, Advanced Synthetic Aperture Radar; SAR, synthetic aperture radar; WS, wide swath.

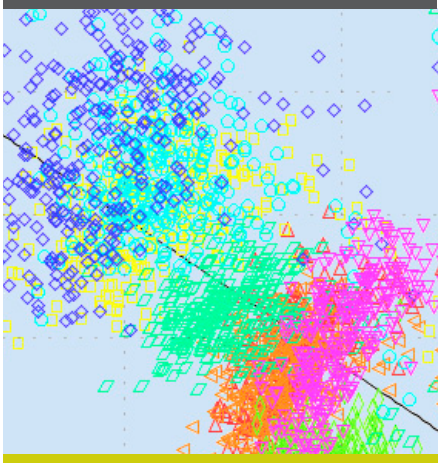

The relationship between the spatial variability of surface soil moisture and the mean surface moisture content is investigated at different scales (field to catchment scale) using in situ measurements and synthetic aperture radar retrievals. We show that the spatial variability strongly depends on scale as well as on soil moisture status.

Dep. of Geography, Univ. of Cologne, Albertus-Magnus-Platz, 50923 Cologne, Germany. *Corresponding author (karl.schneider@uni-koeln.de).

Vadose Zone J. 9:1014–1024
doi:10.2136/vzj2009.0165
Received 18 Nov. 2009.
Published online 7 Sept. 2010.

© Soil Science Society of America
5585 Guilford Rd. Madison, WI 53711 USA.
All rights reserved. No part of this periodical may be reproduced or transmitted in any form or by any means, electronic or mechanical, including photocopying, recording, or any information storage and retrieval system, without permission in writing from the publisher.

Soil moisture and its distribution in space and time plays a critical role in the surface energy balance at the soil–atmosphere interface; it is a key variable influencing the partitioning of solar energy into latent and sensible heat flux as well as the partitioning of precipitation into runoff and percolation. In situ measurements of soil moisture are time and cost intensive. Due to their large spatial variability, estimation of spatial patterns of soil moisture from field measurements is rather difficult and not feasible for large-scale analyses. Although hydrologic models have shown their capability to derive spatial soil moisture patterns, their application is a challenging task, requiring a multitude of input data (such as soil properties, i.e., hydraulic characteristics and permeability, along with meteorologic and climatologic data). Neither the full spatial variability of these environmental parameters nor the full details of the processes are typically known, thus modeled spatial patterns tend to reduce spatial variability. Therefore, as well as due to the need for independent validation, direct and repeatable soil moisture measurements covering large spatial scales obtained from remote sensing instruments is becoming increasingly necessary and now, with the advent of new sensor generations, feasible.

The sensitivity of the radar backscattering coefficient (σ^0) to soil moisture at low microwave frequencies is well described in the literature (Boisvert et al., 1997; Loew et al., 2003; Quesney et al., 2000). Numerous research activities performed within the last three decades have demonstrated that sensors operating in the low-frequency portion of the microwave electromagnetic spectrum (especially the P and L bands) are suitable for measuring the surface moisture content. The penetration depth of the radar beam depends on soil characteristics and moisture state. It is typically in the order of some tenths of the wavelength up to half a wavelength. While the combination of different frequencies, polarizations, and incidence angles provide best results (e.g., Dubois et al., 1995; Wang et al., 1997; Romshoo et al., 2000), these data are today only available from airborne sensors. The P band is not available from current satellite sensors and full polarimetric space-borne L-band data are available only from PALSAR aboard the Advanced Land Observing Satellite (ALOS). Space-borne systems do not offer the repetition rate, spatial resolution, frequency, and polarimetric

characteristics needed for continuous high-resolution soil moisture monitoring. Current and future satellite-based synthetic aperture radar (SAR) systems such as ALOS-2 (Japanese Aerospace Exploration Agency), SENTINAL-1 (European Space Agency), DESDynI (NASA Jet Propulsion Laboratory), etc., are, and will be in the foreseeable future, limited to a single frequency band. Nonetheless, considerable effort has been successfully devoted to research on the retrieval of soil moisture from C-band data, which is operational today on Earth Observation platforms such as ERS-2, RADARSAT-1, ENVISAT, and RADARSAT-2. Besides being sensitive to soil moisture, however, the radar backscatter signal at the C-band (4–8 GHz) is significantly influenced by vegetation and surface roughness. Thus the estimation of spatial soil moisture patterns with a suitable accuracy for many applications requires the use of correction procedures for vegetation and roughness effects (Calvet et al., 1995; Cognard et al., 1995; Le Hégarat-Mascle et al., 2002; Baghdadi et al., 2002; Loew et al., 2006; Bryant et al., 2007).

For bare soils, the relationship between the SAR backscattering coefficient (σ^0), surface roughness, and surface soil moisture has been well investigated (Autret et al., 1989; Calvet et al., 1995; Boisvert et al., 1997; Le Toan et al., 2002; Baghdadi et al., 2002). It is based on the large contrast of the dielectric constant (ε') of dry soil (~3) and water (~80). The dielectric constant directly affects the backscatter intensity. Physically based backscatter models are available for bare soil conditions (Oh et al., 1992; Fung, 1994; Dubois et al., 1995; Baghdadi and Zribi, 2006). In general, these scattering models calculate σ^0 as a function of sensor configuration and soil surface state, allowing the inversion of near-surface volumetric water content; however, these physically based models require either detailed knowledge of the spatial patterns of soil parameters (e.g., surface roughness) or multiple radar channels or polarizations to isolate the effects of the surface dielectric constant and surface roughness. A suitable parameterization of these models, especially for larger areas, is therefore often not possible (Romshoo et al., 2000; van Zyl and Kim, 2001). Empirical and semiempirical algorithms have shown their potential to derive soil moisture from single-frequency SAR data (Oh et al., 1992; Rombach and Mauser, 1997). Their applicability might be limited to the region where they were developed, however, and thus must be validated if transferred to a different area. A comprehensive overview of existing theoretical, semiempirical, and empirical inversion approaches was given by Verhoest et al. (2008).

A key issue with regard to soil moisture is to understand the spatial patterns at different scales, the scaling behavior, and the processes that lead to spatial patterns. Several studies have investigated the spatial variability of soil moisture based on remotely sensed as well as ground-based measurements. Reynolds (1970) classified the controls into static (e.g., topography and soil texture) or dynamic (e.g., rainfall and varying vegetation cover) parameters. The lower boundary of the wilting point and the upper boundary of soil saturation provide physical limits for variations in water content for a given soil texture. Thus, one can assume that the relationship between the spatial variance in soil moisture and the average moisture content shows a decrease in variance at low as well as at high soil moisture values.

Measurements provided by Famiglietti et al. (1998), for instance, support this assumption. They monitored time series of soil moisture along a 200-m hillslope transect and found that the magnitude of the spatial variability across the transect decreased with decreasing mean moisture values. Owe et al. (1982), as well as Albertson and Montaldo (2003), found the trend of variability to depend on the mean soil moisture state. Comparable findings were also published by other groups (e.g., Bell et al., 1980; Western and Grayson, 1998; Choi and Jacobs, 2007). Nevertheless, studies with contradictory observations can be found. Hawley et al. (1983), as well as Charpentier and Groffman (1992), did not find a relationship between mean soil moisture and soil moisture variability. Other researchers found increasing moisture variability with decreasing mean soil moisture (e.g., Famiglietti et al., 1999; Hupet and Vanclooster, 2002; Oldak et al., 2002). These observations indicate that in a complex landscape, the spatial variability is a result of the interactions of many different parameters and processes. Moreover, observations have been made that show that the dependency of the soil moisture variability on the mean soil moisture varies with spatial scale (Rodriguez-Iturbe et al., 1995; Crow and Wood, 1999). Teuling and Troch (2005) showed that both soil and vegetation controls can cause either the creation or destruction of spatial variance. Vereecken et al. (2007) conducted a re-examination of recent experimental work (e.g., Choi and Jacobs, 2007; Choi et al., 2007) showing that the spatial variance increases when drying occurs from a very wet state. Spatial variability peaks at moisture values in the mid range between maximum and minimum values and decreases accordingly with further drying.

The primary aim of the study was to analyze the spatial variability of surface soil moisture based on remote sensing and field measurements at different spatial scales. To this end, we derived a time series of surface soil moisture patterns from ASAR data of the European Earth Observation satellite ENVISAT using an empirical soil moisture retrieval algorithm by Loew et al. (2006). The algorithm was validated with independent ground-truth measurements. Based on these data, the dependence of spatial soil moisture variability on the soil moisture state was analyzed for different spatial scales ranging from the field to the catchment scale.

Materials and Methods

Study Site

The research area of the SFB/TR32, namely the catchment of the River Rur, is located in the western part of Germany, covering a total area of 2364 km^2 with about 10% belonging to Belgium (140 km^2) and the Netherlands (100 km^2). The area is divided into two major landscape units: (i) a fertile loess plain in the north dominated by agriculture, and (ii) a low mountain range in the south characterized by forest and grassland patches (Fig. 1).

Field measurements were performed at two test sites within the catchment. The test site Rollesbroich (50°37′25″ N, 6°18′16″ E) represents typical grassland within the rolling topography of the Eifel. This test site is characterized by a mean elevation of ~510 m above sea level, slopes from 0 to 10° and mean annual precipitation of 1200 mm. The dominant soils are Inceptisols, Alfisols, and Aqualfs developed in silt loam, according to the U.S. Soil Taxonomy. Due to the dense root network of the grass cover, the amount of soil organic matter in the topsoil (<5 cm) is up to 8% (w/w) (Korres et al., 2009). Thus, low bulk densities (0.57–0.83 g cm^{-3}) prevail. The test site Selhausen (50°52′10″ N, 6°27′4″ E) represents an intensively used agricultural area of the Belgium–Germany loess belt (subsequently referred to as fertile loess plain). Crops are grown on virtually flat terrain (slopes 0–4°, mean elevation ~100 m above sea level, mean annual precipitation 705 mm). The major soils are Alfisols and Inceptisols with a silt loam texture.

Ground-truth measurements were taken on 15 sampling fields at the two test sites. The measurements were performed on different land cover types (sugarbeet [*Beta vulgaris* L.], winter wheat [*Triticum aestivum* L.], and grassland vegetation dominated by a ryegrass society, particularly perennial ryegrass [*Lolium perenne* L.] and smooth meadow grass [*Poa pratensis* L.]). The size of the individual sampling fields varied between 2 and 10 ha. The surface soil moisture measurements were arranged in a grid with a sampling point spacing of 30 to 60 m, with 12 to 24 points per field. According to the length of the rods of the hand-held frequency domain reflectometry probes (ThetaProbe ML2x, Delta-T Devices, Cambridge, UK), the measured surface soil moisture was an average value for the topmost 6 cm. To minimize sampling errors and to yield a representative value for each sampling location, each sampling location was represented by the mean of six individual measurements taken within a radius of 40 cm of the sampling location. Obvious measurement errors, which might occur for instance by incomplete contact with the substrate, were excluded from further analysis. At the grassland test site, distributed field measurements were performed during Envisat overflights on 29 April, 3 June, and 16 September. At the arable land test site, distributed surface soil moisture measurements were performed during Envisat overflights on 29 April, 3 June, 8 July, 27 July, and 16 September. In addition, we used measurements from six continuous soil moisture stations installed at the test sites. At these stations, soil water content was monitored with FDR probes installed at 10- and 30-cm depth for grassland, sugarbeet, and winter wheat. A transect along the slope at the Rollesbroich site was observed with a time domain reflectometry (TDR) station (TDR-100/SDMX50, Campbell Scientific, Logan, UT).

Envisat Advanced Synthetic Aperture Radar Data

Envisat ASAR operates at C-band with a center frequency of 5.331 GHz and can perform multiple acquisition modes. The platform revolves around the Earth on a sun-synchronous polar orbit with a nominal reference mean altitude of 800 km and 98.55° inclination. The SAR data used in the present study are eight WS images with a resolution of approximately 150 m and a swath width of 400 km. All images are from 2008, starting on 19 February and ending on 21 October. Because every scene was acquired on the same orbit, the time lag between the single-mode images equals the orbital repeat cycle of 35 d. An overview of the eight ASAR images used is given in Table 1. We used Level 1 ASAR wide-swath single-look complex (ASA_WSS_1P) data, which represent single-look, complex, slant-range, digital images generated from Level 0 data.

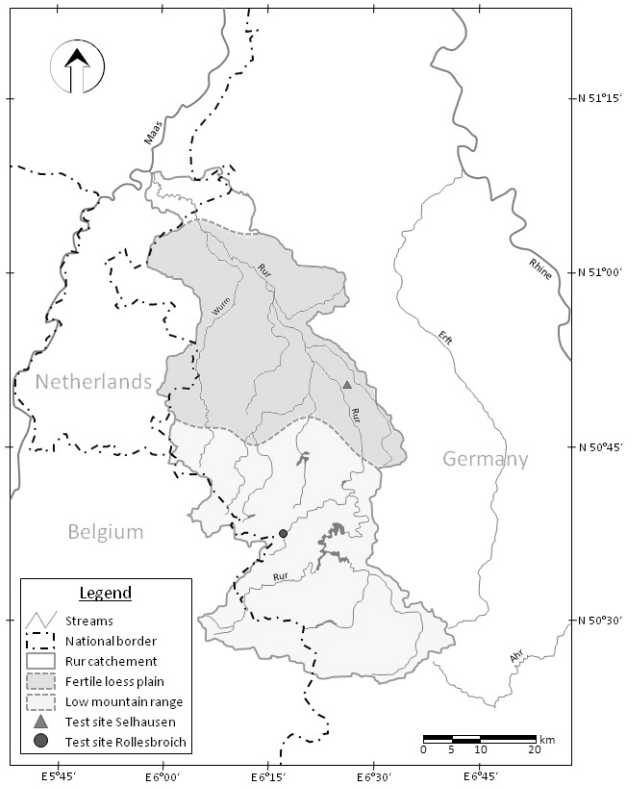

Fig. 1. River Rur catchment with the two major landscape units (gray shaded) and locations of the test sites for in situ soil moisture measurements in Selhausen and Rollesbroich.

Table 1. Overview of the Advanced Synthetic Aperture Radar (ASAR) wide-swath, single-look (WSS), vertically co-polarized data acquired on descending orbits in 2008 used for this study.

Date	Start time	LIA near range†	LIA far range‡	LIA mid range§
	h	°		
19 Feb.	0959:09	28.8	30.5	27.1
25 Mar.	0959:10	28.7	30.4	27.0
29 Apr.	0959:07	28.8	30.5	27.1
3 June	0959:09	28.8	30.5	27.1
8 July	0958:49	28.9	30.6	27.2
12 Aug.	0959:10	28.8	30.5	27.1
16 Sept.	0958:45	28.8	30.5	27.1
21 Oct.	0959:08	28.9	30.6	27.2

† The local incidence angle (LIA) of the very eastern part of the catchment, which is closest to the sensor in range direction.
‡ The LIA of the very western part of the catchment, representing the location farthest from the sensor in range direction.
§ The LIA of the median of the catchment.

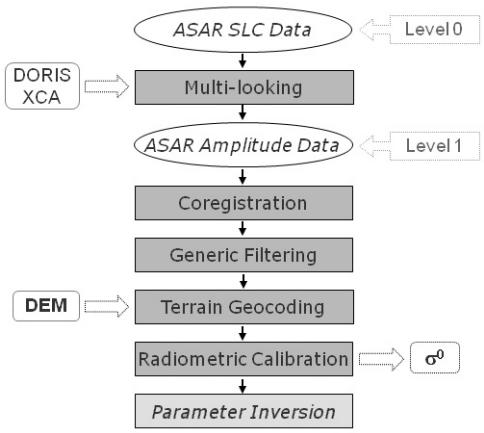

Fig. 2. Basic processing chain for Envisat satellite Advanced Synthetic Aperture Radar (ASAR) wide-swath, single-look complex (SLC) data, with input from external calibration (XCA) data and a digital elevation model (DEM) and output of the radar backscattering coefficient (σ^0).

All images were vertically co-polarized and were acquired on descending orbits.

Advanced Synthetic Aperture Radar Data Processing

There is no standard processing chain for SAR data. Principally, the processing depends on how the data were acquired (SAR system and acquisition mode). Additionally, the type of product that is envisaged determines how intermediate SAR products (i.e., terrain geocoded backscattering coefficient data) will be further processed. All image processing performed in this study used ENVI (ITT Visual Information Solutions, Boulder, CO) and the add-on module SARscape (sarmap, Purasca, Switzerland). Figure 2 outlines the image processing steps.

After header analysis, full resolution extraction is performed to produce single-look complex (SLC) images. Wide-swath data must be multi-looked separately for each of its five subswaths to produce the slant range intensity image with square resolution cells. The resolution of the WS SLC is 150 m. Auxiliary orbit and calibration information for each ASAR image are used to yield the most accurate multi-looked intensity images (Rosich and Meadows, 2004). The DORIS (Doppler Orbitography and Radiopositioning Integrated by Satellite) data provide precise orbital information for Envisat ASAR; two different versions are available. We used the verified orbits (VOR) because they provide the most precise location information; however, VOR data are not available until 1 mo after the actual satellite acquisition at the earliest. In addition, the most recent external calibration data (XCA) files were used to assure the best radiometric accuracy (ESA, 2007). These ancillary ASAR data are also used in the following processing steps.

To render the application of a multitemporal speckle filter and to assure completely identical geometries, the multi-look images were subsequently co-registered. This step requires spatial registration to correct for relative translational shift and rotational and scale differences. Co-registration can be described as the process of superimposing, in the slant range geometry, two or more SAR images having the same acquisition geometry (Meijering and Unser, 2004).

Speckle, a typical feature of SAR images, was reduced in a two-step approach. A first step to reduce the speckle is inherently performed as part of the multi-looking procedure through averaging the range or azimuth resolution cells to produce the spatial resolution of the WS images. According to De Grandi et al. (1997), multitemporal speckle filtering should be applied whenever two or more images of the same scene taken at different times are available. By exploiting the varying temporal correlation of speckle between images, this filtering process significantly reduces the noise. Hence, we used a multitemporal De Grandi filter for despeckling of the images (De Grandi et al., 1997).

After despeckling, the images were geocoded and radiometrically calibrated to σ^0. The SAR images were orthorectified using a high-resolution (10-m) airborne laser scanner digital elevation model (Scilands, 2008). Local terrain slopes and aspects with respect to the incident wave result in significant radiometric as well as geometric distortions in the recorded backscatter amplitude (Meier et al., 1993). Also, the effects of variations in the scattering area must be accounted for (Ulander, 1996; Small et al., 2004). These terrain effects were corrected, including an incidence angle correction, before calculating the surface soil moisture using SARscape.

Empirical Soil Moisture Retrieval Model

The inversion approach for Envisat ASAR data was developed with the aim to provide soil moisture maps for mesoscale catchments in an operational manner. The algorithm is based on an empirical inversion scheme initially developed for C-band SAR data from the European Remote Sensing satellite mission (Rombach and Mauser, 1997). The approach calculates the real part of the complex dielectric constant ε' as a function of land use. Thus the algorithm requires a detailed land use map as well as additional soil texture information for the inversion of ε' to soil moisture by means of a dielectric mixing model. The model has proven its applicability in different studies showing that surface soil moisture contents can be derived with a RMSE of 4 to 7% (v/v) and that it is also usable for mesoscale C-band SAR data (Schneider and Oppelt, 1998; Mauser, 2000; Loew et al., 2003). An advantage of this empirical retrieval approach is that it requires very few model parameters to derive surface soil moisture values. The soil moisture retrieval model has been developed and validated for a range of land cover types, in particular cereal, root crops, bare soils, harvested fields, and grassland. Soil moisture is derived from the remotely measured backscatter in a two-step approach. First, ε' is derived from the SAR backscattering coefficient σ^0 and ancillary land use information. In a second step, the conversion of ε' to volumetric soil moisture (m_v) contents is calculated on the basis of a soil texture map using the dielectric mixing model proposed by Hallikainen et al. (1985).

The measured backscattering coefficient is converted to the relative dielectric constant by

$$\varepsilon' = a + b\sigma^0\,[\mathrm{dB}] + c\sigma^0\,[\mathrm{dB}]^2 \quad [1]$$

where a, b, and c are empirical land-use-dependant model parameters, as shown in Table 2.

In contrast to the constant vegetation influence for the field crops, a significant impact of biomass on the backscattering coefficient was observed for grassland (Rombach and Mauser, 1997). This finding was supported by Dubois et al. (1995), who observed significant differences in backscatter intensities between grassland fields with the same soil moisture content attributable to varying amounts of biomass. Rombach and Mauser (1997) proposed the use of an attenuation factor Ω, which is related to the dry biomass of the grassland vegetation M_{DRY} (kg/m^2) as

$$\Omega = \alpha - \beta\sqrt{M_{DRY}} \quad [2]$$

where α and β are specific parameters, given in Table 2 for intensively and extensively used grassland (Loew et al., 2006). It should be mentioned that the actual physical scattering mechanisms and attenuation properties due to interactions between aboveground biomass, thatch, and the underlying mineral soil constitutes a major problem for the estimation of soil moisture under grassland vegetation from C-band SAR (Martin et al., 1989; Saatchi et al., 1994; Wang et al., 1997). The applicability of an empirical inversion algorithm to a different region and sensor system must be validated with independent measurements. In the present study, this validation was carried out on the basis of a large number of field measurements.

Table 2. Land-use-dependent coefficients for the inversion of the radar backscattering coefficient (σ^0) to the dielectric constant (ε') using Eq. [1] and biomass correction coefficients for Eq. [2] at an incidence angle of 23° (Loew et al., 2006).

Land use	Model parameters			
	a	b	C	R^2
Bare soil	34.20	4.42	0.15	0.90
Cereal	42.77	4.91	0.16	0.88
Harvested fields	45.71	5.87	0.20	0.81
Grassland	40.94	5.33	0.18	0.92
Root crops	42.05	4.42	0.15	0.84
Biomass correction	a	b		
Meadow, extensive use	0.9765	0.7278		
Meadow, intensive use	1.0350	0.5934		

Analysis of Soil Moisture Variability

To analyze the soil moisture variability at different spatial scales, field and remote sensing data with different aggregation levels were used in a three-step approach:

1. In a first step, the ASAR soil moisture retrievals were analyzed at the scale of the entire Rur catchment and at the scales of the two major landscape units. At these scales, differences in soil moisture variability should result from variations in soil, topography (especially in the low mountain range area), land cover type, and potential variations in the spatial distribution of antecedent rainfall

2. In a next step, we analyzed 1.5- by 1.5-km boxes (10 by 10 pixels) of the ASAR-derived soil moisture (the number of boxes per image was 293). This analysis was restricted to the fertile loess plain because the effects of topography on rainfall, soil type, and soil moisture, as well as small-scale patterns in land cover type, should be reduced as far as possible. The mean soil moisture and variance for the 1.5- by 1.5-km boxes were calculated by shifting a nonoverlapping, moving, 10- by 10-pixel window over the ASAR images. Because not all of the pixels in the image (e.g., built-up areas, forests, and water) represent a soil moisture value, only those boxes that had at least 30% of the pixels classified were included in the analysis. At this spatial scale, soil moisture differences should be dominated by differences in land cover type, while differences due to varying soil texture should be small and homogenous antecedent rainfall is still a reasonable assumption.

3. For a field-scale evaluation, the field measurements at Selhausen were analyzed on the basis of individual fields (0.02–0.10 km^2) to address the within-field soil moisture variability because differences in soil texture were small and homogenous antecedent rainfall per field could be assumed.

At all spatial scales, the soil moisture variability was compared with the mean soil moisture content. To avoid interdependency between both statistical moments, coefficients of variation instead of standard deviations were used to represent variability.

Results and Discussion

Soil Moisture Retrievals

Eight WS images were processed for 2008. As an example, Fig. 3 shows the spatial patterns and frequency distribution of the soil moisture map for 25 March. Areas where the land cover did not allow the calculation of the surface soil moisture (e.g., built-up areas, forests, and water) remain unspecified in the soil moisture maps. The soil moisture frequency distribution of the derived pattern is shown in the histogram. The histogram shows a bimodal soil moisture distribution averaging 34.5% (v/v), with a range of 25 to 47.5% (v/v); the first and second peaks are centered at 31.5 and 38% (v/v), respectively. While the soil moisture map shows quite similar soil moisture values within the major landscapes units, it can be seen that the low mountain range part is wetter than most areas of the fertile loess plain. Within a period of 2 d before the satellite overpass, the catchment received precipitation amounts ranging from 2.2 to 8.5 mm. The image covers 97% of the Rur catchment area. The southeastern part of the catchment (approximately 70 km^2) is not covered due to missing land use information.

To evaluate the applicability and quality of the derived soil moisture inversion algorithm, we compared the surface soil moisture values calculated from the ASAR data with in situ ground-truth measurements.

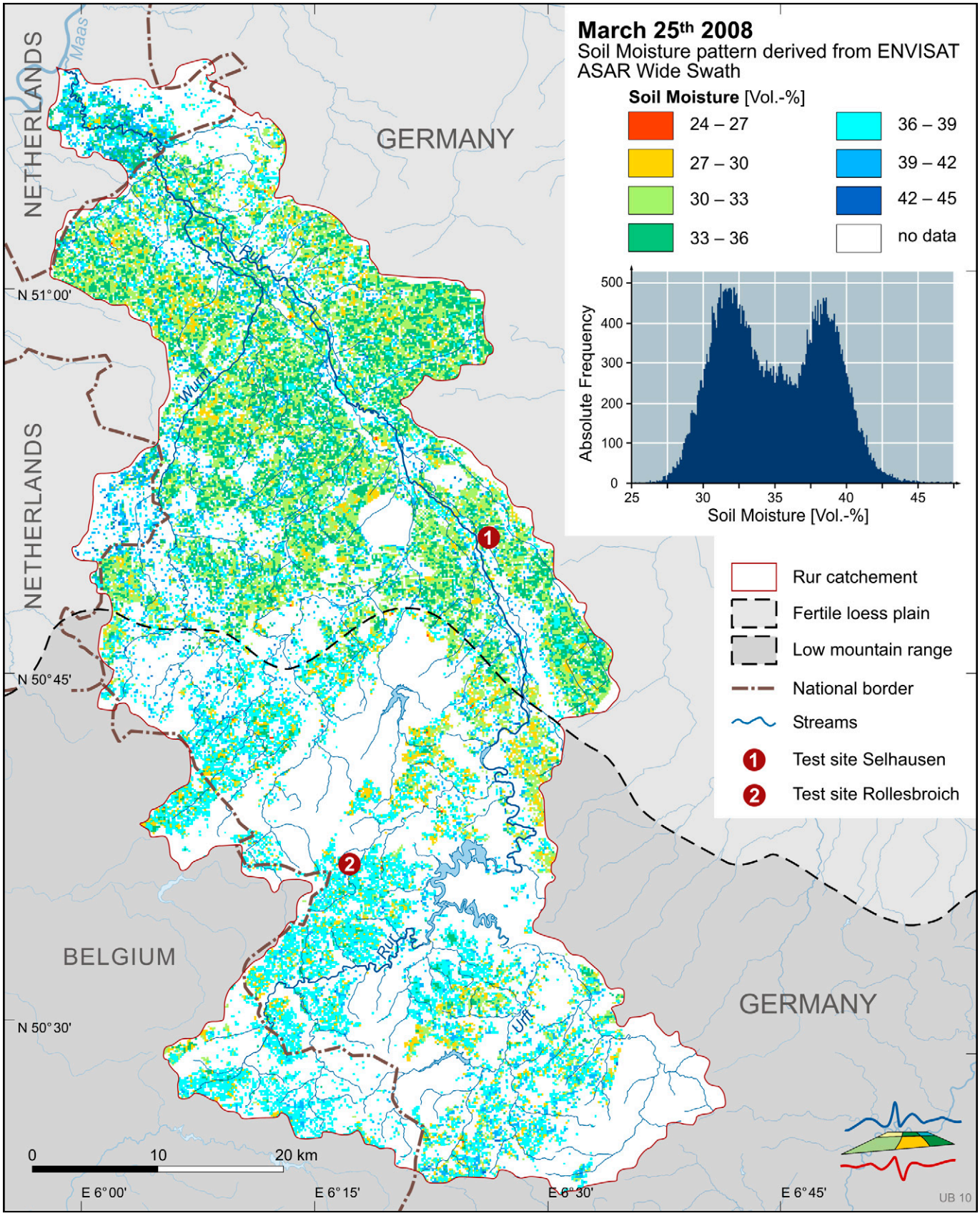

Fig. 3. Envisat satellite Advanced Synthetic Aperture Radar (ASAR) derived soil moisture pattern of the River Rur catchment from 25 Mar. 2008.

The soil moisture estimates were determined on a pixel-by-pixel basis from the space-borne microwave measurements in the C-band using the empirical algorithm discussed above. Because the coefficients of these equations were based on previous research (Rombach and Mauser, 1997), ground-truth data and remote sensing estimates were independent of each other. Because ASAR WS pixels provide an average value for a 150- by 150-m surface, comparison of remote sensing and ground measurement was done on the basis of individual fields and for all available dates with ground-truth data.

Figure 4 shows the comparison of measured and retrieved soil moisture values for all eight maps. Triangles indicate the average values measured for the different fields. According to the individual size, each field is represented by 10 to 24 measurement locations, each covered by six samples. In addition, measurements taken at our continuous-measurement sites are shown as circles. Because the continuous measurements represent only the given measurement location instead of an areal average, larger differences in the point measurements and the spatial mean covered by the remote sensing data may exist. Nevertheless, the measurements taken at the continuous-measurement sites match the values derived from remote sensing very well.

Comparison of the field average ground-truth data with ASAR-derived soil moisture values yielded a RMSE of 5% (v/v). While field measurements and remote sensing estimates agreed well in the mid and low soil moisture range, at high soil moisture states the ASAR retrievals significantly underestimated the field measurements. Very high soil moisture values in excess of 45% (v/v) were measured only under grassland, where the handheld probes integrated the wet thatch and the mineral soil parts. The thatch layer of the grass cover and the organic topsoil layer provided a large storage capacity for water, which exceeded the porosity of the mineral soils and thereby dominated the soil moisture measurement. The empirical inversion algorithm did not appropriately account for this effect. In addition, the soil texture map did not reflect the large water retention characteristic of the organic upper layer of this land use–soil combination. For dry conditions, the soil moisture estimates for grassland as well as for arable land agreed well with the field measurements. This indicates that for dry conditions, the measured water content of the soil is mainly determined by the properties of the mineral soil rather than the thatch layer.

The soil moisture conditions of the arable land of the loess plain were generally well represented by the ASAR estimates. Because the inversion algorithms were developed mainly for mineral soils, they performed well here. If field-measured soil moisture values >45% (v/v) are excluded from the comparison and thereby the effect of the organic topsoil layer reduced, a RMSE of 4.3% (v/v) is achieved. Loew et al. (2006) pointed out that the empirical model is based on a limited set of observations, representing a span of 18 and 45% (v/v) and thus might be less accurate beyond this range.

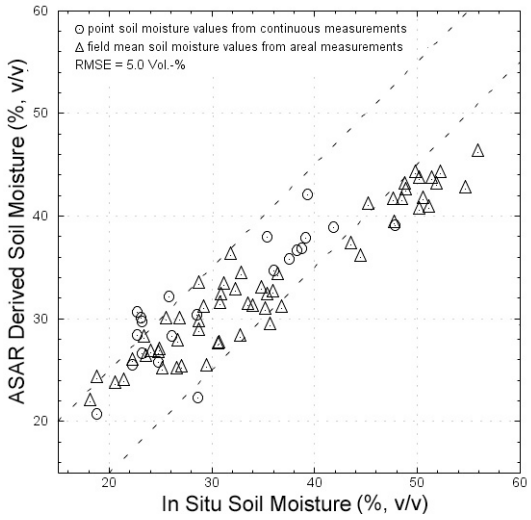

Fig. 4. Comparison between measured and Advanced Synthetic Aperture Radar (ASAR) derived surface soil moisture. Field soil moisture values are averages from 10 to 24 individual measurement locations. Dashed lines indicate the ±5% (v/v) margins.

Nevertheless, one has to be aware of different sources of uncertainty in the estimation of surface soil moistures from ASAR data, which can arise from the following:

1. Image calibration errors, which range between 0.5 and 1.0 dB for the ASAR products (ESA, 2007). Insufficient speckle reduction can add a stochastic component to σ^0. Both error sources were assumed to be small because accurate ancillary data and state-of-the-art image processing were used.

2. Imprecise land use information and land use specific conversion, which can result in a false inversion of σ^0 to ε'.

3. Unknown or imprecise biomass information for grassland pixels. Spatial variability in biomass results in spatial variability of the attenuation factor. We used field measurements to determine the biomass of the grassland. While these measurements provided accurate data for our sample fields, they might not be accurate everywhere in the catchment.

4. Unknown or imprecise soil texture information, which can result in a false conversion of ε' to volumetric soil moisture by means of dielectric mixing models.

Analysis of Soil Moisture Variability

The relationship between the mean soil moisture and the CV calculated for the whole Rur watershed using all ASAR soil moisture images is shown in Fig. 5. The CV decreased linearly with increasing mean soil moisture. A decreasing soil moisture variability with increasing soil moisture has been described in the literature (e.g., Famiglietti et al., 1999; Hupet and Vanclooster, 2002; Choi et al., 2007) and should be expected, particularly when areas with homogeneous soil textures approach saturation.

As described above, the watershed consists of two distinctively different regions: the flat loess plain and the mountainous Eifel region. Land use and soil textures as well as their spatial variability are

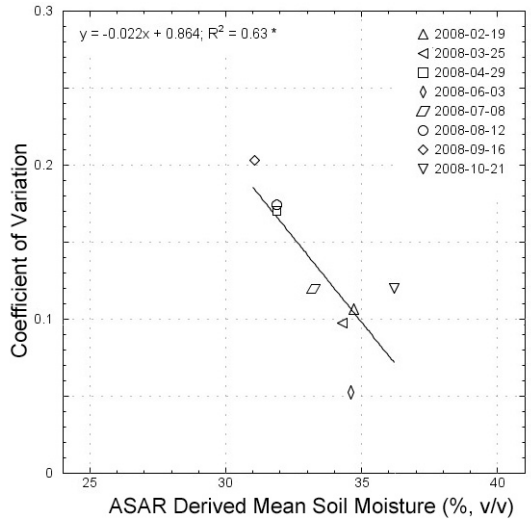

Fig. 5. Relationship between Advanced Synthetic Aperture Radar (ASAR) derived mean soil moisture and the CV for the entire River Rur catchment.

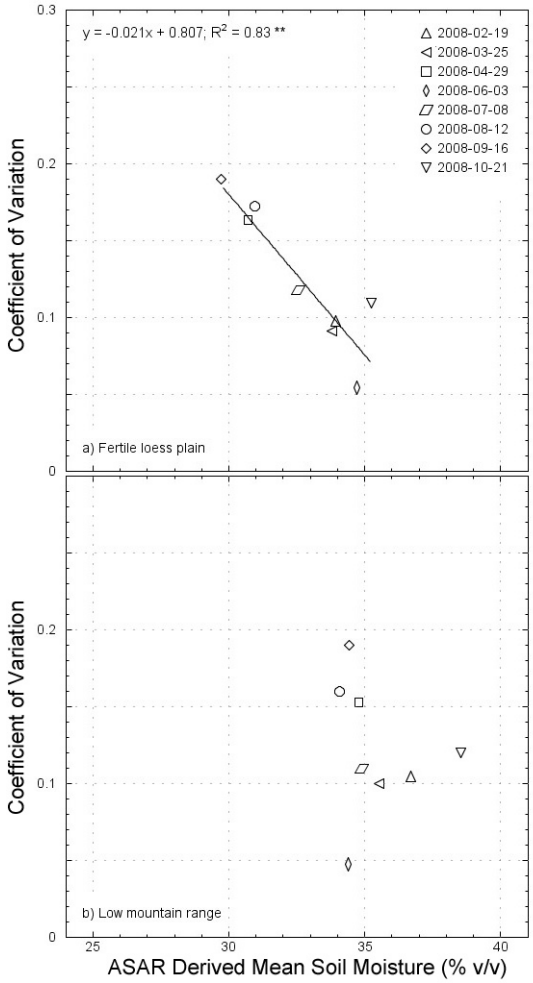

Fig. 6. Relationship between Advanced Synthetic Aperture Radar (ASAR) derived soil moisture and the CV for (a) the fertile loess plain, and (b) the low mountain range region.

significantly different in both regions. While in the Eifel region the topography results in large spatial heterogeneity, particularly with respect to soil texture, the loess plain exhibits more or less uniform soil textures but differs strongly with respect to different types of arable land use. These differences in landscape properties may result in a different relationship between average soil moisture and soil moisture variability. Consequently, we analyzed this relationship separately for both regions (Fig. 6).

The correlation for the loess plain (Fig. 6a) yielded a very strong negative relationship ($R^2 = 0.83$) between the mean soil moisture and the spatial moisture variability as expressed by the CV. The slope of the relationship is very close to the slope for the whole catchment. In contrast, the relationship for the Eifel area does not show a clear trend (Fig. 6b). Even at high soil moisture levels, the spatial variability was high. While the soil texture in the loess plain is rather uniform, the soil textures in the Eifel vary considerably, from mineral soils saturating at moisture values between 45 and 50% (v/v) to organic soil or soils with an organic topsoil layer with surface soil moisture values in excess of 60% (v/v). Thus, even at or close to saturation, the Eifel soils showed large spatial variability. Moreover, the hilly topography of the Eifel also caused larger spatial variation in precipitation.

Figure 7 shows the relationship of the CV and the mean surface soil moisture based on 10- by 10-pixel boxes for the fertile loess plain. The different acquisition dates of the images are color coded to allow assessment of the variability with a given scene. The slope of the regression line in Fig. 7 is significantly smaller than the respective slope for the whole area (Fig. 6a). While the soil moisture varied considerably within the 10 by 10 box for all soil moisture values, the decrease in the CV with increasing soil moisture described above is still obvious. In addition, the upper limit of the soil moisture variability decreased significantly with increasing soil moisture and the lower limit of the soil moisture variability within the 10 by 10 boxes was considerably larger at lower soil moistures than at soil moistures in excess of 32% (v/v).

Figure 8 shows the relationship between the mean field surface soil moisture measured during our field campaigns and the CV within the individual fields. It can be seen that the CV decreased again with increasing mean soil moisture. For the soil moisture range from 15 to 34% (v/v), the linear regression resulted in a coefficient of determination of 0.59 and a slope of −0.0063 on the winter wheat fields, and a coefficient of determination of 0.76 and a slope of −0.0065 on the sugarbeet fields. At the field scale, the slope of the regression line is significantly smaller than the slope for the mesoscale (10- by 10-pixel boxes) or the regional scale. Thus, while the level of spatial variation shows a comparable range of values at all spatial scales, the decrease in the soil moisture variability with increasing soil moisture was smaller at the local scale than at the large scale.

Choi and Jacobs (2007) also used an exponential fit as an efficient way to explain soil moisture variability patterns as a function of mean

soil moisture. An exponential fit CV = $A\exp(B\theta)$ between mean soil moisture and CV yields a tighter coefficient of determination of 0.60 with $A = 0.521$ and $B = -0.059$, and of 0.81 with $A = 0.591$ and $B = -0.073$ for the winter wheat and sugarbeet fields, respectively. The parameter A describes the relative variability range and B indicates the variability change as related to mean soil moisture. Hence, parameter A is related to the maximum relative variability while parameter B is related to the slope of the relative variability. The parameters A and B, as observed from our in situ field measurements, are consistent with the observations of surface soil moisture variability from the Small Explorer (SMEX), as reported by Choi et al. (2007).

The negative correlations between soil moisture variability and mean soil moisture content found in our study are consistent with previous studies of Famiglietti et al. (1999), Hupet and Vanclooster (2002), and Choi and Jacobs (2007). Nonetheless, it should be noted that some studies also found positive relationships between the mean surface soil moisture content and the soil moisture variability (Famiglietti et al., 1998; Western and Grayson, 1998). These studies postulated that variability peaked under wet conditions because soil heterogeneity would be maximized after precipitation events. While we concur that spatially heterogeneous precipitation, particularly when investigating large areas, results in increased heterogeneity if soil saturation is not reached, our findings indicate that for areas with homogeneous soil textures, the soil moisture variability decreases with increasing soil moisture. In regions with large differences in soil texture and thus soil porosity and maximum soil moisture values at saturation, however, this relationship might not hold and may result in a large soil moisture variability even at high soil moistures, as evidenced by the data for the Eifel. According to Famiglietti et al. (1998), the combined effects of soil texture, hysteresis effects, vegetation, topography, and sampling scale may lead to different relationships between spatial variability and soil moisture.

Figure 9 provides a comprehensive overview of the relationship of spatial soil moisture variability and soil moisture values for different spatial scales. As can be seen, the gain of the relationship between soil moisture value and CV decreases with scale. Hence, at a given soil moisture level, we observed the highest variability at the scale of the entire Rur catchment and the smallest variability at the field scale. We attribute this to the fact that the drivers of variations in surface soil moisture contents are much more variable at the larger scale. If we consider precipitation as the dominant driving process for spatial variance on days with high mean soil moisture values, the variability in surface soil water contents increases with increasing scale because the amounts of rainfall, with annual means of ~600 mm in the fertile loess plain and >1200 mm in the low mountain range, vary significantly across the whole Rur catchment. At smaller scales, on the other hand, these fluctuations in precipitation decrease and contribute only small amounts of variance. On days with dry conditions, i.e., low mean soil moisture values, variance is more likely driven by processes associated with evapotranspiration. Thus, soil moisture

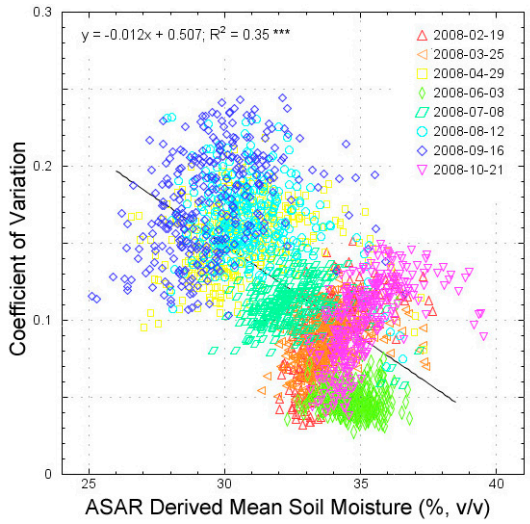

Fig. 7. Relationship between Advanced Synthetic Aperture Radar (ASAR) derived soil moisture and the CV for (a) the fertile loess plain pixels taking into account all dates and land cover classes.

variability also increases with increasing scale due to the fact that spatial heterogeneities of factors like soil clay content, vegetation (including agricultural management), and topographic conditions become larger the larger the scale.

As microwave remote sensing using the C-band only provides information about the top surface layer of a soil volume, it is unclear if these relationships also hold for deeper soil layers. Thus, care should be taken in extrapolating statistics from surface measurements (e.g., SAR) to the entire root zone. Choi and Jacobs (2007) found that surface soil moisture had the least negative relationship (slope closest to zero) between CV and mean soil moisture in comparison to deeper soil layers. According to them, these small variability patterns for the surface layer are affected by the high

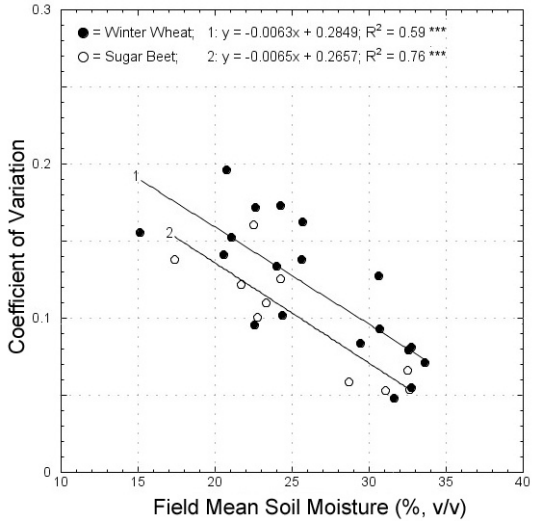

Fig. 8. Relationship between field mean soil moisture and the CV from in situ measurements at the Rollesbroich and Selhausen test sites.

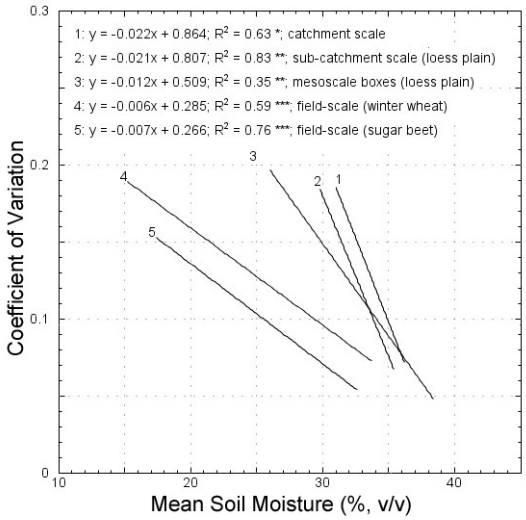

Fig. 9. Overview of the scale-dependent relationships between the CV and the mean surface soil moisture.

variation in mean soil moisture at the surface. Several other studies found less variability at deeper depths compared with surface soil moisture observations (Famiglietti et al., 1999; Hupet and Vanclooster, 2002; Albertson and Montaldo, 2003).

Conclusions

An empirical retrieval algorithm of surface soil moisture from Envisat ASAR data in the C-band was applied successfully within the Rur catchment. We validated the model to derive soil moisture values for a catchment in central Europe yielding a RMSE of 5.0% (v/v). The main advantage of the inversion scheme is that it requires very few parameters in comparison with other retrieval approaches. With regard to the operational use of any parameter inversion model for either optical or microwave remote sensing data, the availability of input parameters is of great importance. The highest deviations from in situ values of the derived soil moisture were recorded on wet meadows and a mature sugarbeet field. The model parameters could be further improved using empirical data measured under these conditions; however, any improvement of the algorithm will rely on a better assessment of the vegetation influence on the C-band backscattering mechanisms, taking into account dynamic vegetation effects.

The variability of mean surface soil moisture was investigated at different scales using in situ measurements and eight ASAR-derived soil moisture patterns. By analyzing the relationships between the spatial variance and the mean soil moisture state at the scales of the entire catchment (~2400 km^2), the two major landscape units (~1000 km^2), boxes (2.25 km^2), and individual fields (~0.1 km^2), we found that the CVs decreased with decreasing sampling scale for all data sets. The different slopes of the linear correlations, ranging from −0.0063 at the field scale to −0.022 at the catchment scale, indicate that small-scale and large-scale variances depend differently on mean soil moisture content.

Acknowledgments

We gratefully acknowledge financial support by the SFB/TR-32 "Patterns in Soil–Vegetation–Atmosphere Systems: Monitoring, Modeling, and Data Assimilation" funded by the German Research Foundation (DFG). In addition, we thank the European Space Agency (ESA) for the provision of Envisat ASAR data through their PI program (AOALO.3570).

References

Albertson, J., and N. Montaldo. 2003. Temporal dynamics of soil moisture variability: 1. Theoretical basis. Water Resour. Res. 39(10):1274, doi:10.1029/2002WR001616.

Autret, M., R. Bernard, and D. Vidal-Madjar. 1989. Theoretical study of the sensitivity of the microwave backscattering coefficient to the soil surface parameters. Int. J. Remote Sens. 10:171–179.

Baghdadi, N., C. King, A. Chanzy, and J.P. Wigneron. 2002. An empirical calibration of the integral equation model based on SAR data, soil moisture, and surface roughness measurements over bare soils. Int. J. Remote Sens. 23:4325–4340.

Baghdadi, N., and M. Zribi. 2006. Evaluation of radar backscatter models IEM, OH and Dubois using experimental observations. Int. J. Remote Sens. 27:3831–3852.

Bell, K.R., B.J. Blanchard, T.J. Schmugge, and M.W. Witzak. 1980. Analysis of surface moisture variations within large-field sites. Water Resour. Res. 16:796–810.

Boisvert, J.B., Q.H.J. Gwyn, A. Chanza, D.J. Major, B. Brisco, and R.J. Brown. 1997. Effect of soil surface moisture gradients on modelling radar backscattering from bare fields. Int. J. Remote Sens. 18:153–170.

Bryant, R., M.S. Moran, D.P. Thoma, C.D. Holifield, S. Skirvin, and M.M. Rahman. 2007. Measuring surface roughness to parameterize radar backscatter models for retrieval of surface soil moisture. IEEE Geosci. Remote Sens. Lett. 4:137–141.

Calvet, J.-C., J.-P. Wigneron, A. Chanzy, S. Raju, and L. Laguerre. 1995. Microwave dielectric properties of a silt-loam at high-frequencies. IEEE Trans. Geosci. Remote Sens. 33:634–642.

Charpentier, M., and P. Groffman. 1992. Soil moisture variability within remote sensing pixels. J. Geophys. Res. 97:18,987–18,995.

Choi, M., and J.M. Jacobs. 2007. Soil moisture variability of root zone profiles within SMEX02 remote sensing footprints. Adv. Water Resour. 30:883–896.

Choi, M., J.M. Jacobs, and M.H. Cosh. 2007. Scaled spatial variability of soil moisture fields. Geophys. Res. Lett. 34:L01401, doi:10.1029/2006GL028247.

Cognard, A.L., C. Loumagne, M. Normand, P. Olivier, C. Ottlé, D. Vidal-Madjar, S. Louahala, and A. Vidal. 1995. Evaluation of the ERS-1/synthetic aperture radar capacity to estimate surface soil moisture: Two year results over the Naizin watershed. Water Resour. Res. 31:975–982.

Crow, W.T., and E.F. Wood. 1999. Multi-scale dynamics of soil moisture variability observed during SGP'97. Geophys. Res. Lett. 26:3485–3488.

De Grandi, G.F., M. Leysen, J.S. Lee, and D. Schuler. 1997. Radar reflectivity estimation using multiple SAR scenes of the same target: Techniques and applications. p. 1047–1050. *In* IGARSS '97: Remote Sensing, A Scientific Vision for Sustainable Development, Singapore. 3–8 Aug. 1997. Vol. 2. IEEE, New York.

Dubois, P.C., J.J. van Zyl, and T. Engman. 1995. Measuring soil moisture with imaging radar. IEEE Trans. Geosci. Remote Sens. 33:915–926.

European Space Agency. 2007. ASAR product handbook issue 2.2. ESA, Paris.

Famiglietti, J., J. Devereaux, C. Laymon, T. Tsegaye, P. Houser, T. Jackson, S. Graham, M. Rodell, and P. Oevelen. 1999. Ground-based investigation of soil moisture variability within remote sensing footprints during the Southern Great Plains 1997 (SGP97) hydrology experiment. Water Resour. Res. 35:1839–1851.

Famiglietti, J., J. Rudnicki, and M. Rodell. 1998. Variability in surface moisture content along a hillslope transect: Rattlesnake Hill, Texas. J. Hydrol. 210:259–281.

Fung, A.K. 1994. Microwave scattering and emission models and their applications. Artech House, Boston.

Hallikainen, M.T., F.T. Ulaby, M.C. Dobson, M.A. El-Rayes, and L.-K. Wu. 1985. Microwave dielectric behavior of wet soil: I. Empirical models and experimental observations. IEEE Trans. Geosci. Remote Sens. 23:25–34.

Hawley, M., T. Jackson, and R. McCuen. 1983. Surface soil moisture variation on small agricultural watersheds. J. Hydrol. 62:179–200.

Hupet, F., and M. Vanclooster. 2002. Intraseasonal dynamics of soil moisture variability within a small agricultural maize crop field. J. Hydrol. 261:86–101.

Korres, W., C.N. Koyama, P. Fiener, and K. Schneider. 2009. Analysis of surface soil moisture patterns in agricultural landscapes using empirical orthogonal functions. Hydrol. Earth Syst. Sci. Discuss. 6:5565–5601.

Le Hégarat-Mascle, S., M. Zribi, F. Alem, A. Weisse, and C. Loumagne. 2002. Soil moisture estimation from ERS/SAR data: Toward an operational methodology. IEEE Trans. Geosci. Remote Sens. 40:2647–2658.

Le Toan, T., M. Davidson, F. Mattia, P. Borderies, I. Chenerie, and T. Manninen. 2002. Improved observation and modeling of bare soil surface for soil moisture retrieval. p. 20–24. *In* Retrieval of Bio- and Geophysical Parameters from SAR Data for Land Applications: Proc. Int. Symp., 3rd, Sheffield, UK, 11-14 Sept. 2001. ESA SP-475. Eur. Space Agency, Paris.

Loew, A., R. Ludwig, and W. Mauser. 2003. Mesoscale soil moisture estimation from SAR data using subscale land use information. p. 1396–1398. *In* IGARSS '03 Proc., Toulouse, France. 21–25 July 2003. Vol. 2. IEEE, New York.

Loew, A., R. Ludwig, and W. Mauser. 2006. Derivation of surface soil moisture from Envisat ASAR wide swath and image mode data in agricultural areas. IEEE Trans. Geosci. Remote Sens. 44:889–899.

Martin, R.D., G. Asrar, and E.T. Kanemasu. 1989. C-band scatterometer measurements of a tallgrass prairie. Remote Sens. Environ. 29:281–292.

Mauser, W. 2000. Comparison of ERS SAR data derived soil moisture distributions with SVAT model results. *In* Proc. ERS-Envisat Symp.: Looking Down to Earth in the New Millennium, Gothenburg, Sweden [CD-ROM]. ESA-SP461. Eur. Space Agency, Paris.

Meier, E., U. Frei, and D. Nuesch. 1993. Precise terrain corrected geocoded maps. p. 173–185. *In* G. Schreier (ed.) SAR processing: Data and systems. Wichmann, Karlsruhe, Germany.

Meijering, E., and M. Unser. 2004. A Note on cubic convolution. IEEE Trans. Image Process. 12:477–479.

Oh, Y., K. Sarabandi, and F.T. Ulaby. 1992. An empirical model and an inversion technique for radar scattering from bare soil surfaces. IEEE Trans. Geosci. Remote Sens. 30:370–381.

Oldak, A., T.J. Jackson, and Y. Pachepsky. 2002. Using GIS in passive microwave soil moisture mapping and geostatistical analysis. Int. J. Geogr. Inf. Sci. 16:681–698.

Owe, M., E. Jones, and T. Schmugge. 1982. Soil moisture variation patterns observed in Hand County, South Dakota. Water Resour. Bull. 16:949–954.

Quesney, A., S. Le Hégarat-Mascle, O. Taconet, D. Vidal-Madjar, J.-P. Wigneron, C. Loumagne, and M. Normand. 2000. Estimation of watershed soil moisture index from ERS/SAR data. Remote Sens. Environ. 72:915–926.

Reynolds, S.G. 1970. The gravimetric method of soil moisture determination: III. An examination of factors influencing soil moisture variability. J. Hydrol. 11:188–200.

Rodriguez-Iturbe, I., G.V. Vogel, R. Rigon, D. Entkhabi, F. Castelli, and A. Rinaldo. 1995. On the spatial organization of soil moisture fields. Geophys. Res. Lett. 22:2757–2760.

Rombach, M., and W. Mauser. 1997. Multi-annual analysis of ERS surface soil moisture measurements of different land uses. p. 703–708. *In* Space at the Service of the Environment: Proc. ERS Symp., 3rd, Florence, Italy. ESA SP414. Eur. Space Agency, Paris.

Romshoo, S.A., T. Nakaegawa, T. Oki, and K. Musiake. 2000. Estimation of soil moisture using spaceborne SAR data and scattering models. *In* Proc. Remote Sens. Soc. Japan Conf., 28th, Tsukuba. 19–21 May 2000. Remote Sens. Soc. of Japan, Tokyo.

Rosich, B., and P. Meadows. 2004. Absolute calibration of ASAR Level 1 products generated with PF-ASAR. ESA ESRIN, Frascati, Italy.

Saatchi, S.S., D.M. Le Vine, and R.H. Lang. 1994. Microwave backscattering and emission model for grass canopies. IEEE Trans. Geosci. Remote Sens. 32:177–186.

Schneider, K., and N. Oppelt. 1998. Determination of mesoscale soil moisture patterns with ERS data. pp. 1831–1833. *In* IGARSS '98: IEEE Int. Geosci. and Remote Sens. Symp., Seattle, WA. 6–10 July 1998. IEEE, New York.

Scilands. 2008. Dokumentation zur Aufbereitung eines DGM10 für das Rur-Gebiet. Scilands GmbH, Göttingen, Germany.

Small, D., M. Jehle, E. Meier, and D. Nuesch. 2004. Robust radiometric terrain correction for SAR image comparison. p. 929–932. *In* Proc. EUSAR 2004: Eur. Conf. on Synthetic Aperture Radar, 5th, Ulm, Germany. 25–27 May 2004. VDE Verlag, Berlin.

Teuling, A.J., and P.A. Troch. 2005. Improved understanding of soil moisture variability dynamics. Geophys. Res. Lett. 32:L05404, doi:10.1029/2004GL021935.

Ulander, L.M. 1996. Radiometric slope correction of synthetic aperture radar images. IEEE Trans. Geosci. Remote Sens. 34:1115–1122.

van Zyl, J.J., and Y.J. Kim. 2001. A quantitative comparison of soil moisture inversion algorithms. p. 37–39. *In* Scanning the Present and Resolving the Future: Proc. IEEE 2001 Int. Geosci. and Remote Sens. Symp., Sydney, Australia. 9–13 July 2001. IEEE, New York.

Vereecken, H., T. Kamai, T. Harter, R. Kasteel, J. Hopmans, and J. Vanderborght. 2007. Explaining soil moisture variability as a function of mean soil moisture: A stochastic unsaturated flow perspective. Geophys. Res. Lett. 34:L22402, doi:10.1029/2007GL031813.

Verhoest, N.E.C., H. Lievens, W. Wagner, J. Álvarez-Mozos, M.S. Moran, and F. Mattia. 2008. On the soil roughness parameterization problem in soil moisture retrieval of bare surfaces from synthetic aperture radar. Sensors 8:4213–4248.

Wang, J., A. Hsu, J.C. Shi, P. O'Neil, and T. Engman. 1997. Estimating surface soil moisture from SIR-C measurements over Little Washita River watershed. Remote Sens. Environ. 59:308–320.

Western, A., and R. Grayson. 1998. The Tarrawara data set: Soil moisture patterns, soil characteristics, and hydrological flux measurements. Water Resour. Res. 34:2765–2768.